

RSC Advances



This is an *Accepted Manuscript*, which has been through the Royal Society of Chemistry peer review process and has been accepted for publication.

Accepted Manuscripts are published online shortly after acceptance, before technical editing, formatting and proof reading. Using this free service, authors can make their results available to the community, in citable form, before we publish the edited article. This *Accepted Manuscript* will be replaced by the edited, formatted and paginated article as soon as this is available.

You can find more information about *Accepted Manuscripts* in the [Information for Authors](#).

Please note that technical editing may introduce minor changes to the text and/or graphics, which may alter content. The journal's standard [Terms & Conditions](#) and the [Ethical guidelines](#) still apply. In no event shall the Royal Society of Chemistry be held responsible for any errors or omissions in this *Accepted Manuscript* or any consequences arising from the use of any information it contains.



Experimental and Theoretical Investigations of *Michelia Alba* Leaves Extract as a Green Highly-effective Corrosion Inhibitor for Different Steel Materials in Acidic Solution

Received 00th January 20xx,
Accepted 00th January 20xx

DOI: 10.1039/x0xx00000x

www.rsc.org/

Lingjie Li^a, Wenting Xu^a, Jinglei Lei^{a*}, Junying Wang^a, Jianxin He^a, Nianbing Li^b, Fusheng Pan^c

The aqueous *Michelia alba* leaves extract (MALE) was first evaluated as an inhibitor to corrosion of different steel materials (industrial pure iron, stainless steel and carbon steel) in hydrochloric acid. The adsorption and corrosion inhibition of MALE were investigated by potentiodynamic polarization, scanning electron microscopy (SEM), Fourier transform infrared spectroscopy (FTIR) and quantum chemical calculations. The results showed that MALE acted as a highly-efficient mixed-type inhibitor for all steels and increasing temperature benefited its corrosion inhibition. The adsorptions of MALE on steel surfaces obeyed Langmuir adsorption isotherm. Quantum chemical calculation results provided reasonable theoretical explanation for the inhibition property of MALE.

Introduction

Steels, e.g. industrial pure iron, stainless steel, carbon steel and etc., have wide applications in industries. All steels are apt to serious corrosion when they contact with acid solutions such as hydrochloric acid and sulfuric acid during acid pickling and cleaning processes.¹⁻⁴ To protect steels from acid corrosion, many methods have been utilized, among which inhibitor is one of the most facile and effective methods.⁵ The traditional inhibitors, such as synthetic organic compounds, are very effective in reducing corrosion of steels. However, most of them are expensive and highly toxic to both human beings and environment. Thus, the development and application of corrosion inhibitors are focused on the inexpensive and environmental-friendly substances. The plant extracts emerge out as green effective corrosion-inhibitors in recent years because of their low-cost, high availability, high biodegradability, and non-toxic nature.^{6,7} The leaves extracts of *occimum viridis*,¹ *hibiscus sabdariffa*,¹ *thyme*,⁸ *ochrosia oppositifolia*,⁹ *acalypha torta*¹⁰ and *piper guineense*,¹¹ barks extracts of *ochrosia oppositifolia*⁹ and *schinopsis lorentzii*,¹² seed extracts of *phoenix dactylifera*,¹³ root extract of *chlorophytum borivilianum*,¹⁴ flowers extracts of *artemisia pallens*¹⁵ and *tagetes erecta*¹⁶ were reported as good inhibitors

for mild-steel corrosion in aggressive acid solutions. The extracts of coffee ground,¹⁷ fruit peels,¹⁸ garlic peels,¹⁹ *oxandra asbeckii* leaves,²⁰ and *osmanthus fragran* leaves^{2,21} were found to display strong inhibition for carbon-steel corrosion in acid solutions. The leaves extracts of ginkgo²² and bamboo^{3,4} were regarded as good corrosion inhibitors for cold-rolled steel in acid solutions and that of *salvia officinalis*²³ showed effective inhibition to the corrosion of stainless steel in hydrochloric acid solution. Obviously, these reported plant inhibitors can protect one certain steel from acid corrosion. However, to the best of our knowledge, no plant inhibitor has been reported to have general highly-efficient inhibition to acid corrosion of different steel materials. Therefore, developing new plant inhibitors with general highly-effective inhibition to corrosion of different steel materials in acid solutions is highly desirable in industrial applications.

Michelia alba is a member of the *magnoliaceae* family of flowering plants, which are well known for the aroma constituents and bioactivities.^{24,25} Though the flowers of *M. alba* have demonstrated great economic importance, the leaves of *M. alba* have been rarely utilized and always treated as wastes. Constituents of *M. alba* leaves have been reported to include aporphines, oxoaporphines, sesquiterpenes, terpenes, benzenoids, steroids, and lignans as well as some aliphatic compounds such as palmitic acid, stearic acid, and linoleic acid,²⁶ which are rich in functional groups with oxygen and nitrogen atoms, epoxy groups and aromatic rings that meet the general structural consideration of corrosion inhibitors.^{6,7,27-29} Hence, it is inferred that *M. alba* leaves may find important application in corrosion inhibition.

In the present work, *M. alba* leaves extract (MALE) is first evaluated as a corrosion inhibitor for three different types of steel materials (industrial pure iron, stainless steel and carbon steel) in hydrochloric acid. The adsorption and corrosion

^a School of Chemistry and Chemical Engineering, Chongqing University, Chongqing, 400044 PR China;

^b School of Chemistry and Chemical Engineering, Southwest University, Chongqing, 400715 PR China;

^c School of Materials Science and Engineering, Chongqing University, Chongqing, 400044 PR China

* Jinglei Lei. Tel.: +86 13983064116; Fax: +86 23 65112328; E-mail address: JLLei@cqu.edu.cn.

† Electronic Supplementary Information (ESI) available: See DOI: 10.1039/x0xx00000x

inhibition of MALE are investigated by the potentiodynamic polarization method, scanning electron microscopy (SEM), Fourier transform infrared spectroscopy (FTIR) and quantum chemical calculations in detail. Such work on exploiting the utility of *M. alba* leaves in inhibition of steel corrosion is hopeful to expand the industrial applications of *M. alba* leaves and to develop new green inhibitors with more effective and general inhibition for acid-corrosion of different steel materials.

Results and discussion

Polarization curves

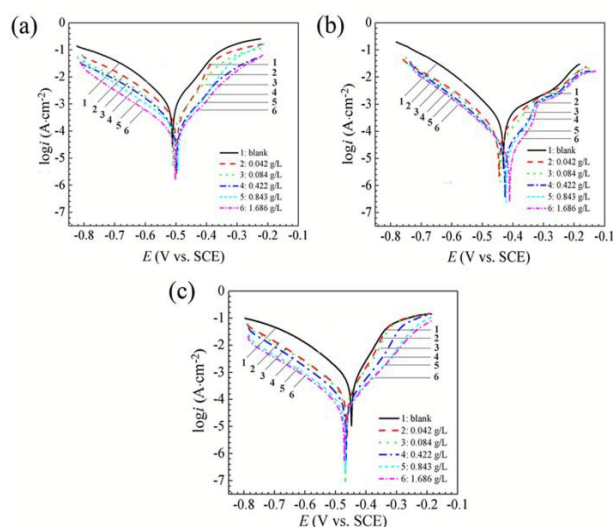


Fig. 1 Polarization curves of (a) industrial-pure iron, (b) 303 stainless steel, and (c) Q235 carbon steel in 1.0 M HCl with different concentrations of MALE at 20 °C.

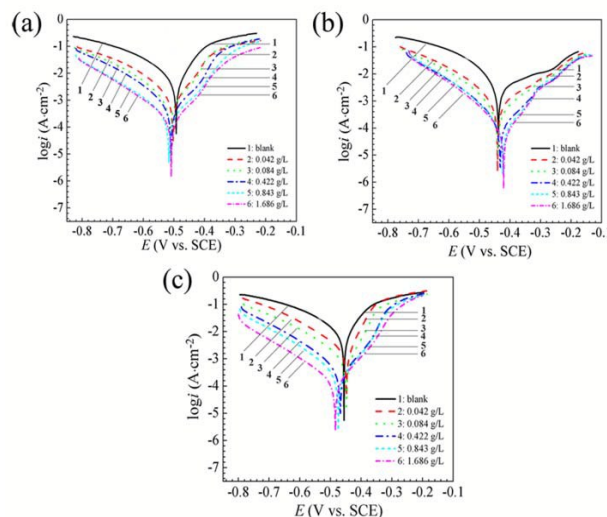


Fig. 2 Polarization curves of (a) industrial-pure iron, (b) 303 stainless steel, and (c) Q235 carbon steel in 1.0 M HCl with different concentrations of MALE at 40 °C.

Figs. 1 and 2 illustrate the polarization curves of industrial-pure iron (a), 303 stainless steel (b) and Q235 carbon steel (c) in 1.0M HCl solutions containing different concentrations of MALE at T_1 (20 °C) and T_2 (40 °C), respectively. The inhibition efficiency (η) can be calculated using the following equation:

$$\eta = \frac{i_{\text{corr}} - i_{\text{corr}'}}{i_{\text{corr}}} \times 100\% \quad (1)$$

where i_{corr} and $i_{\text{corr}'}$ are the corrosion current densities respectively in the absence and presence of MALE, determined by extrapolation of the cathodic Tafel lines to the corrosion potential.

Table 1 Parameters obtained from potentiodynamic polarization plots in Fig. 1.

Steel materials	C_{MALE} (g L ⁻¹)	E_{corr} (mV vs. SCE)	b_c (mV dec ⁻¹)	b_a (mV dec ⁻¹)	i_{corr} ($\mu\text{A cm}^{-2}$)	η (%)
Industrial-pure iron	0	-512	-103	68	1033	—
	0.042	-498	-114	50	403	61.0
	0.084	-510	-114	64	318	69.2
	0.422	-498	-111	74	198	80.8
	0.843	-494	-125	65	150	85.5
	1.686	-502	-127	83	102	90.2
303 stainless steel	0	-431	-93	143	257	—
	0.042	-445	-99	104	113	56.0
	0.084	-441	-94	76	70	73.0
	0.422	-426	-95	65	38	85.2
	0.843	-422	-95	58	31	87.9
	1.686	-411	-97	58	22	91.5
Q235 carbon steel	0	-448	-109	57	583	—
	0.042	-463	-118	47	186	68.1
	0.084	-467	-117	54	181	69.0
	0.422	-465	-113	68	106	81.8
	0.843	-468	-117	88	69	88.1
	1.686	-471	-113	86	54	90.8

Table 2 Parameters obtained from potentiodynamic polarization plots in Fig. 2.

Steel materials	C_{MALE} (g L ⁻¹)	E_{corr} (mV vs. SCE)	b_c (mV dec ⁻¹)	b_a (mV dec ⁻¹)	i_{corr} (μA cm ⁻²)	η (%)
Industrial-pure iron	0	-493	-141	78	6194	—
	0.042	-515	-123	61	1435	76.8
	0.084	-503	-121	66	964	84.4
	0.422	-510	-119	80	584	90.6
	0.843	-517	-126	81	268	95.7
	1.686	-509	-128	76	205	96.7
303 stainless steel	0	-438	-125	189	5358	—
	0.042	-441	-117	168	904	83.1
	0.084	-440	-111	137	538	90.0
	0.422	-432	-107	88	196	96.3
	0.843	-424	-97	72	129	97.6
	1.686	-421	-99	69	101	98.1
Q235 carbon steel	0	-456	-156	91	8851	—
	0.042	-448	-140	80	1991	77.5
	0.084	-449	-134	56	991	88.8
	0.422	-468	-124	78	402	95.5
	0.843	-475	-124	75	292	96.7
	1.686	-484	-130	82	138	98.4

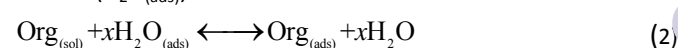
At both temperatures, the presence of MALE shifts both cathodic and anodic branches to the lower values of corrosion current densities and thus causes a remarkable decrease in the corrosion rate for the three different steel materials. The parameters, corrosion potential (E_{corr}), Tafel slopes (b_c and b_a), corrosion current density (i_{corr}) and inhibition efficiency (η) that derived from the polarization curves in Figs. 1 and 2 are given in Tables 1 and 2, respectively. As well known, different steel materials have dissimilar chemical compositions and microstructures, which result in their different corrosion behavior in acid solutions. Apparently, among the three types of steel materials, stainless steel is the least corrosive material while industrial-pure iron shows most serious corrosion at 20 °C and carbon steel shows most serious corrosion at 40 °C. However, regardless of steel types, i_{corr} decreases considerably in the presence MALE and the inhibition efficiencies η are higher than 90% at 20 °C and 96% at 40 °C, which indicates that MALE is a highly-efficient inhibitor with general inhibition for different steel materials in acid solution.

The parallel cathodic polarization curves in Figs.1 and 2 suggest that the hydrogen evolution is activation-controlled and the reduction mechanism is not affected by the presence of MALE.^{13,30,31} The anodic current decreases in the presence of MALE compared to its absence, which implies that MALE can also suppress the anodic dissolution of steels. Generally, an inhibitor can be classified as cathodic or anodic type if the shift of corrosion potential is more than 85mV with respect to that in the inhibitor absence.^{13,30–32} From Figs.1 and 2 together with Tables 1 and 2, the maximum shift of E_{corr} is far less than 85mV in the presence of MALE compared to its absence, which suggests that MALE acts as a mixed-type inhibitor. From the

above results, it can be deduced that the inhibition of MALE might base upon the adsorption of its constituent molecules at the steel/solution interfaces while affect little on the mechanism of either the anodic metal dissolution or the cathodic hydrogen evolution reaction.

Adsorption behaviors

Generally, the adsorption process of organic molecules at a metal/solution interface can be regarded as the following replacement process of water molecules on the metallic surface ($\text{H}_2\text{O}_{(\text{ads})}$).³³



where $\text{Org}_{(\text{sol})}$ and $\text{Org}_{(\text{ads})}$ are the organic molecules respectively in the solution and adsorbed on the metallic surface; x represents the number of water molecules replaced by organic molecules absorbed. Thus, the inhibition mechanism of MALE can be explained on the basis of the adsorption behavior of its constituent molecules. The adsorption isotherm (the variation of surface coverage θ against the inhibitor concentration c) is used to describe the nature of adsorption.³⁴ Several adsorption isotherms, such as Langmuir (c/θ vs c), Frumkin (θ vs c) and Temkin (θ vs $\log c$), are commonly used to characterize the adsorption performance. The following Langmuir adsorption isotherm was found to be the one that best explains the experimental results for MALE:

$$\frac{c}{\theta} = \frac{1}{K_{\text{ads}}} + c \quad (3)$$

where c is the concentration of MALE; K_{ads} is the adsorptive equilibrium constant; and ϑ is the surface coverage of MALE on steel materials, which can be calculated by $\eta/100$.³⁴⁻³⁸

Fig. 3 shows the straight lines of c/ϑ vs. c at T_1 (20 °C) and T_2 (40 °C) for industrial-pure iron (a), 303 stainless steel (b) and Q235 carbon steel (c). Regardless of steel types, the linear correlation coefficients and the slopes are almost equal to 1 at both temperatures, which confirm that the adsorptions of MALE on the three steel surfaces all obey Langmuir adsorption isotherm. Usually, higher values of adsorptive equilibrium constant K_{ads} imply better inhibition efficiency and more efficient adsorption.³⁹ The values of K_{ads} at 40 °C are all higher than those at 20 °C, which implies that the high temperature benefits the strong adsorption of MALE on steel surfaces. Thus, the inhibition efficiencies of MALE at 40 °C are higher than those at 20 °C can be well understood.

Moreover, the adsorption heat can be calculated according to the van't Hoff equation:^{35,36}

$$\ln K = \frac{-\Delta H^\theta}{RT} + \text{const} \quad (4)$$

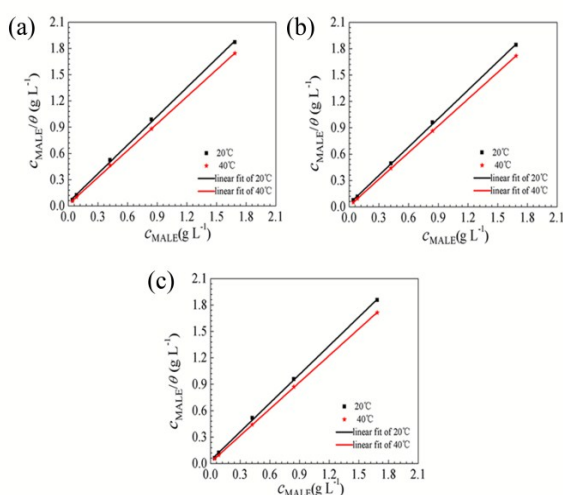


Fig. 3 Adsorption isotherms of MALE on surfaces of (a) industrial-pure iron, (b) 303 stainless steel, and (c) Q235 carbon steel at 20 °C and 40 °C.

Table 3. Linear regression parameters for adsorption of MALE on different steel surfaces and some thermodynamic parameters derived.

Steel materials	Temp. (°C)	R^2	K_{ads} (L g^{-1})	ΔH^θ (kJ mol^{-1})	ΔG^θ (kJ mol^{-1})
Industrial-pure iron	20	0.999	24.9	30.4	-17.6
	40	1.000	55.3	30.4	-20.9
303 stainless steel	20	0.999	29.9	51.8	-18.1
	40	0.999	116.3	51.8	-22.8
Q235 carbon steel	20	0.999	29.3	35.9	-18.0
	40	0.999	75.1	35.9	-21.7

that is:

$$\ln\left(\frac{K_2}{K_1}\right) = \frac{-\Delta H^\theta}{R} \left(\frac{1}{T_2} - \frac{1}{T_1}\right) \quad (5)$$

where ΔH^θ is the adsorption heat, R is the gas constant ($8.314 \text{ J K mol}^{-1}$), T is the absolute temperature, K_1 and K_2 are the adsorptive equilibrium constants at T_1 (20 °C) and T_2 (40 °C), respectively. Because the experiments proceed at the standard pressure and the solution concentrations are not very high, which are close to the standard condition, the calculated adsorption heat thus can be approximately regarded as the standard adsorption heat ΔH^θ .^{2,36} The positive values of ΔH^θ (Table 3) suggest that the adsorptions of MALE on the steel surfaces are endothermic. The standard adsorption free energy (ΔG^θ) can be obtained according to the following equation:^{2,11,34,37}

$$K = \frac{1}{55.5} \exp\left(\frac{-\Delta G^\theta}{RT}\right) \quad (6)$$

The negative values of ΔG^θ (Table 3) indicate that the adsorptions of MALE on the steel surfaces are spontaneous. Generally, the values of ΔG^θ around or less than -20 kJ mol^{-1} are associated with the electrostatic interaction between charged molecules and the charged metal surface (physisorption) while those around or higher than -40 kJ mol^{-1} mean charge sharing or transfer from the inhibitor molecules to the metal surface to form a coordinate type of metal bond (chemisorption).^{2,32,33} The ΔG^θ values for the three different steel materials listed in Table 3 are all around -20 kJ mol^{-1} , which means that the adsorptions of MALE on the steel surfaces belong to physisorption and the adsorptive films have electrostatic characters.^{2,38,39}

SEM results

The surface morphologies of industrial-pure iron (Fig.4a and a'), 303 stainless steel (Fig.4b and b') and Q235 carbon steel (Fig.4c and c') samples after immersion in 1.0 M HCl solution in absence and presence of MALE (1.686 g L^{-1}) for 1 h were examined by SEM and the corresponding images are shown in Fig.4.

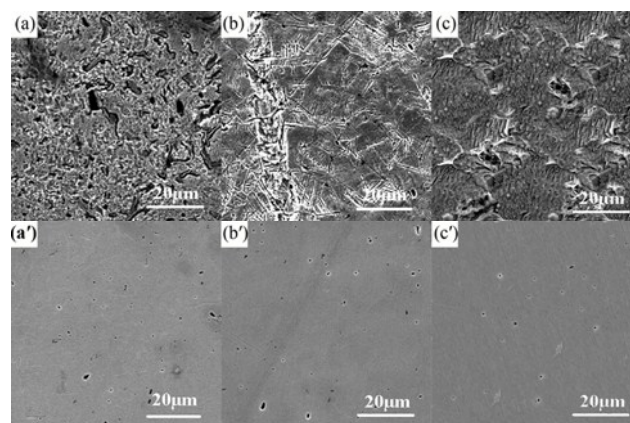


Fig.4. SEM images of surfaces of (a and a') industrial-pure iron, (b and b') 303 stainless steel, and (c and c') Q235 carbon steel after immersion in 1.0 M HCl solution without and (a', b' and c') with 1.686 g L^{-1} MALE for 1 h.

In the absence of MALE (Fig. 4a, b and c), the surfaces of three steels display strongly-damaged morphologies with many pits and cracks, indicating the serious corrosion of steel materials in hydrochloric acid. While in the presence of MALE (Fig. 4a', b' and c'), the surfaces of three steels are much smoother as a consequence of formation of uniform and dense surface films due to adsorption of MALE, which significantly reduce the corrosion rate and provide strong protection for steel materials. These SEM results further confirm the results deduced from the potentiodynamic polarization tests that MALE is a highly-efficient inhibitor for the corrosion of steel materials.

FTIR results

Fig. 5 shows the FTIR spectra of MALE powder (Fig. 5a), and surface films formed on industrial-pure iron (Fig. 5b), 303 stainless steel (Fig. 5c), and Q235 carbon steel (Fig. 5d) after immersion in 1.0 M HCl containing 0.843 g L⁻¹ MALE for 1 h. The corresponding functional groups assigned to the FTIR bands in Fig. 5 are identified in Table S2 in the ESI[†]. From Fig. 5 and Table S2 in the ESI[†], it can be inferred that pure MALE powder contains oxygen and nitrogen atoms in functional groups (O–H, C=O, C–N, C–O, C=C), epoxy group and aromatic ring, which is in agreement with the previous report on constituents of *M. alba* leaves.^{12,34,40–43} These functional groups are always found in constituents of plant corrosion inhibitors, which are considered to be crucial for the inhibition property.^{6,7,27–29} Compared with those of pure MALE powder, the FTIR results of surface films formed on different steel materials display some differences, e.g. some disappearing vibrations and shifting bands. These changes might be due to formation of complex of Fe²⁺-MALE adsorbing on steel surfaces, which is responsible for corrosion inhibition.

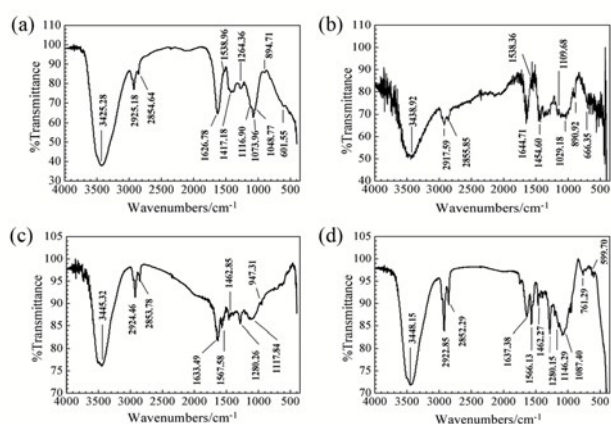


Fig. 5 FTIR spectra of (a) MALE powder, and surface films of (b) industrial-pure iron, (c) 303 stainless steel, and (d) Q235 carbon steel after immersion in 1.0 M HCl containing 0.843 g L⁻¹ MALE for 1 h.

Quantum chemical calculation results

Generally, a plant extract is considered as a complex mixture of various phytochemical components. According to the

previous investigation on constituents of *M. alba* leaves^{24–26} and the above FTIR results, and further after some qualitative tests on inhibition property of each assumed component, gallic acid [GA], flavanoids [Fvo], *p*-hydroxybenzoic acid [*p*-HA] and liriodenine are identified as the major effective components in MALE. Hence, quantum chemical calculations are performed to model the adsorption structures of the above four chemical constituents (GA, Fvo, *p*-HA and liriodenine) in order to provide some insights into the nature of their interactions with steels and their contributions to inhibitions.

Figs. 6 and 7 show the optimized structures, the highest occupied molecular orbitals (HOMO) and the lowest unoccupied molecular orbitals (LUMO) of GA, Fvo, *p*-HA and liriodenine. Clearly, HOMO of the four molecules is predominantly made up of N, O atoms and benzene rings.⁴⁴ Table 4 lists some quantum chemical parameters, which are thought important due to their direct influence on electronic interactions between the inhibitor molecules and steel surfaces. E_{HOMO} , energy of the highest occupied molecular orbital; E_{LUMO} , energy of the lowest unoccupied molecular orbital; ΔE , energy gap between E_{LUMO} and E_{HOMO} ; μ , dipole moment; $\langle \alpha \rangle$, polarizability; η , hardness; σ , softness; Π , electronic chemical potential; χ , electronegativity and ω , electrophilicity index. The η , σ , Π , χ and ω parameters are calculated using the following equations:^{45–48}

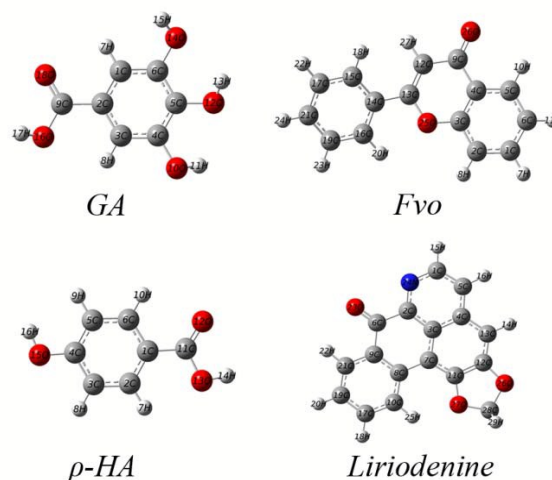


Fig. 6 Optimized structures of molecules of the major effective components of MALE in the neutral form.

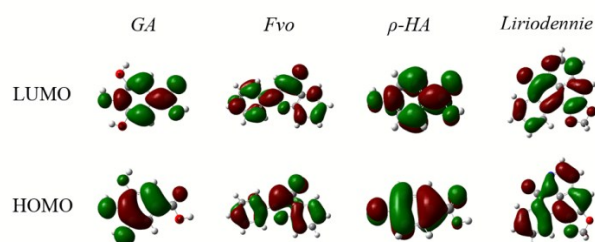


Fig. 7 LUMO and HOMO distribution of the calculated molecules in the neutral form.

$$\eta = \frac{(I - A)}{2} \quad (7)$$

$$\sigma = \frac{1}{\eta} \quad (8)$$

$$-Pi = \frac{(I+A)}{2} = \chi \quad (9)$$

$$\omega = \frac{Pi^2}{2\eta} \quad (10)$$

where

$$I = -E_{\text{HOMO}} \quad (11)$$

$$A = -E_{\text{LUMO}} \quad (12)$$

and a theoretical χ_M value of 7 eV mol⁻¹ and η_M value of 0 eV mol⁻¹ for iron atom.⁴⁸

According to the frontier molecular orbital (FMO) theory,^{27,49} the electron transition is due to an interaction between HOMO and LUMO of the reacting species. E_{HOMO} level is often associated with the electron donating ability of a molecule and the higher E_{HOMO} value usually indicates a tendency of a molecule to donate electrons to the appropriate acceptor molecule with low energy and empty electron orbital. The value of E_{LUMO} is related to the ability of a molecule to accept electrons and the lower E_{LUMO} value often means that the molecule likely accepts electrons. Thus, the ΔE value is regarded as a measure for the stability of a formed complex on metal surface and the lower ΔE value reflects the higher stability of a formed complex.^{27,50} The dipole moment μ is a measure of the polarity of a covalent bond, which is related to the distribution of electrons in a molecule.^{50,51} Generally, the larger μ value favors the adsorption of inhibitor.⁵¹ The polarizability $\langle\alpha\rangle$ is an indicator of the linear response of the electron density in the presence of an infinitesimal electric field, which depends on the second derivative of energy with respect to the electric field.^{44,52} The higher $\langle\alpha\rangle$ value facilitates the strong adsorption process and high inhibition efficiency.⁵² The hardness η and softness σ can also reflect the ability of a molecule to accept and offer electrons. For the simplest transfer of electrons, adsorption could occur at the part of the molecule where σ has the highest value and η has the lowest value.⁵³ The electrophilicity index ω is a measure of the electrophilic power of a molecule, the higher value of which means the higher capacity of a molecule to accept electrons.^{47,53}

From Table 4, the E_{HOMO} values of GA, Fvo, ρ -HA and liriodenine show very small differences (less than 0.42 eV), which indicates that these molecules have similar abilities to donate electrons to metallic surface.⁵⁴ Liriodenine has the lowest E_{LUMO} (-2.40 eV) and ΔE (3.62 eV), which implies the high capacity to accept electrons from the d -orbital of Fe and the high stability of the [Fe–liriodenine] complexes.⁵⁵ Moreover, liriodenine has the highest values of dipole moment μ and polarizability $\langle\alpha\rangle$ among these molecules, which implies the strong adsorption of liriodenine molecules at steel surfaces.

Table 4 Calculated quantum chemical parameters for the major effective components of MALE in the neutral form.

	GA	Fvo	ρ -HA	Liriodenine
E_{HOMO} (eV)	-5.98	-6.34	-6.40	-6.01
E_{LUMO} (eV)	-1.05	-1.79	-1.03	-2.40
ΔE (eV)	4.93	4.55	5.37	3.61
μ (D)	2.41	4.19	1.85	6.94
$\langle\alpha\rangle$	88.01	164.24	79.17	199.56
η (eV)	2.46	2.28	2.68	1.80
σ (eV ⁻¹)	0.41	0.44	0.37	0.56
Pi (eV)	-3.52	-4.06	-3.72	-4.20
χ (eV)	3.52	4.06	3.72	4.20
ω	2.52	3.61	2.58	4.90

As for the η and σ parameters, the lowest η value and highest σ value of liriodenine indicate the highly effective inhibition of liriodenine to steel corrosion, which agrees well with other theoretical reports.^{27,56,57} Liriodenine has the highest ω value, which further confirms its high capacity to accept electrons and adsorb on steel surfaces to inhibit corrosion.

The above calculation results and discussion are propitious to the four major effective components in the neutral form. Further considering that the protonation of those four components might occur in acid medium, the calculations for the protonated form are performed. Figs. S2 and S3 in the ESI† show the optimized structures, the highest occupied molecular orbitals (HOMO) and the lowest unoccupied molecular orbitals (LUMO) of GA, Fvo, ρ -HA and liriodenine in the protonated form. Table S3 in the ESI† lists the related quantum chemical parameters.

It is evident that the protonated form of the four major effective components shows similar tendency to their neutral form. Liriodenine exhibits the highest E_{HOMO} , and the lowest E_{LUMO} and ΔE , suggesting the protonated form is the most likely form for its interaction with steels.^{58–60} Moreover, the protonated liriodenine has the lowest value of hardness η , and the highest value of softness σ and polarizability $\langle\alpha\rangle$, indicating that liriodenine has the best inhibitive performance on the steel surface in the protonated form.^{61,62} Besides, the protonated liriodenine has the highest ω value, confirming that liriodenine in the protonated form is the most reactive inhibitor that can easily adsorb on the steel surface to provide stronger protection.^{15,63} In addition, the protonated GA has the highest values of dipole moment μ among all those four molecules, implying that GA has a good inhibitive performance to steel corrosion in the protonated form. All those results and deductions are in consistent with those calculated in case of the neutral form. However, the protonated ones make greater contribution than their neutral counterparts.

Considering all the calculated parameters and the molecule structures in the neutral and protonated forms, liriodenine is presumed to play the most important role in the inhibition performance of MALE, and Fvo and GA also make big

contributions while ρ -HA has the least inhibition effect. However, since these molecules differ considerably in their chemical structures and any of them might exert a dominant effect under specific conditions and concentrations.

Experimental

Materials and solutions

Tests were performed on three distinct steel materials with obvious different compositions and applications: industrial-pure iron, 303 stainless steel and Q235 carbon steel (Rong Chuang Metal Co., Ltd., Dongguan, PR China). The compositions of the above steel materials are listed in Table S1 of the ESI[†]. The aggressive solution (1.0 M HCl) was prepared by dilution of 37% hydrochloric acid (analytical grade; Sinopharm Chemical Reagent Co., Ltd., Shanghai, PR China) with distilled water.

Fresh *M. alba* leaves (Fig. S1 in the ESI[†]) were picked in the campus of Chongqing University in PR China. The aqueous MALE was prepared in the following way: 60 g fresh *M. alba* leaves were finely shredded and heated in boiled distilled water for 1 h. The mixture was filtered and the clear liquid was concentrated, dried in an oven to gain the dark-brown solid and then ground to obtain the extract powder, whose weight was 7.580 g. The extract powder was then added into the aggressive solution (1.0 M HCl) to prepare the test solutions with the desired MALE concentration. The concentration range of MALE used was 0.042–1.686 g L⁻¹.

Electrochemical measurements

The inhibition efficiency of MALE was evaluated by using potentiodynamic polarization measurements, which were carried out on a CHI760B electrochemical workstation (Shanghai Chenhua Instruments Inc., PR China). The electrochemical cell consisted of a conventional three-electrode configuration with a platinum sheet as the counter electrode, a saturated calomel electrode (SCE) coupled with a Luggin-Haber capillary as the reference electrode, the different steel electrodes as the working electrodes, and 1.0 M HCl solutions with different concentrations of MALE as the electrolytes. The tip of the Luggin capillary was very close to the working electrode surface in order to minimize ohmic contributions. The steel working electrodes were cut from the above three steel rods with cross-section area of 1 cm² and embedded in epoxy resin holders. Before each experiment, the surface of the working electrode was abraded with 200, 600, 800 and 1200# grit emery papers, then degreased ultrasonically in absolute ethanol for 3 min, rinsed with distilled water and dried in air. Before each measurement, the working electrode was immersed in the quiescent test solution (open to air) until the cell open circuit potential (OCP) became stable. The polarization curves were recorded from -0.30 V (vs. OCP) to +0.30 V (vs. OCP) at a sweep rate of 0.5 mV s⁻¹. Each test was repeated more than three times to verify reproducibility of the results.

SEM and FTIR characterizations

The surface morphology of different steel samples after immersion in 1.0 M HCl solution in absence and presence of MALE (with the concentration of 1.686 g L⁻¹) at 20°C for 1 h was examined by a scanning electron microscope (SEM, TESCAN VEGA II LMU, Czech).

FTIR spectra of four specimens were recorded by using a Fourier transform infrared spectrometer (FTIR, Nicolet 60-SXB, USA), which extended from 400 to 4000 cm⁻¹, using the KBr disk technique. One specimen for FTIR characterization was the MALE powder, which was mixed with KBr and made into the disk. Other three specimens were the thin adsorption layers formed on three different steel surfaces after immersion in 1.0 M HCl solution containing 0.843 g L⁻¹ MALE at 20°C for 1 h, which was cleaned and dried first and then rubbed with a small amount of KBr powder and made into the disk.

Quantum chemical calculations

The quantum theoretical calculations were carried out using Gaussian 09 program. The full geometry optimization together with the vibrational analysis of the optimized structures was carried out at the DFT (density functional theory) B₃LYP level using 6-31G* basis set to ensure that the optimized structures were corresponded to the minimum of the potential energy surface (no imaginary frequency). The quantum chemical parameters were then obtained from the optimized structure using 6-31G* basis set in gas phase. It has been proposed that carrying out the theoretical calculations in gas phase is a useful method because the results obtained in gas phase show no remarkable differences from those obtained in liquid phase while it can significantly reduce the time of calculation.⁶⁴⁻⁶⁹

Conclusions

- (1) The electrochemical polarization results indicate that MALE acts as a highly-efficient mixed-type inhibitor for corrosion of different steel materials in acid solution and increasing temperature benefits its corrosion inhibition.
- (2) The adsorptions of MALE on three steel surfaces all obey the Langmuir adsorption isotherm.
- (3) The uniform and dense adsorptive films over three steel surfaces efficiently inhibit the corrosion of steel materials.
- (4) The quantum-chemical calculations are performed by taking into consideration both the protonated and the nonprotonated species, which indicates that the component lirioidenine plays the most important role in the inhibition performance of MALE.

Acknowledgements

The authors acknowledge the financial support from the National Natural Science Foundation of China (21273295, 21373281, 21573028), the Program for New Century Excellent Talents in University (NCET-12-0587, NCET-13-0633), the Project for Distinguished Young Scholars in Chongqing

(cstc2014jcyj100004), the Program of China Scholarships Council (No. 201406055006), the Fundamental Research Funds for the Central Universities (CDJZR13225501, CDJZR14228801) and the sharing fund of Chongqing University's Large-scale Equipment. The authors also thank Prof. Mingli Yang in Institute of Atomic and Molecular Physics of Sichuan University of P.R. China for supporting Gaussian 09 program as well as for the instructive discussion on quantum chemical calculations.

Notes and references

- E. E. Oguzie, *Corros. Sci.*, 2008, **50**, 2993.
- L. J. Li, X. P. Zhang, J. L. Lei, J. X. He, S. T. Zhang, F. S. Pan, *Corros. Sci.*, 2012, **63**, 82.
- X. H. Li, S. D. Deng, H. Fu, X. G. Xie, *Corros. Sci.*, 2014, **78**, 29.
- X. H. Li, S. D. Deng, H. Fu, *Corros. Sci.*, 2012, **62**, 163.
- V. S. Sastri, *Corrosion Inhibitors - Principles and Applications*, first ed., Wiley, New York, 1998.
- P. B. Raja, M. G. Sethuraman, *Mater. Lett.*, 2008, **62**, 113.
- M. Finšgar, J. Jackson, *Corros. Sci.*, 2014, **86**, 17.
- T. Ibrahim, H. Alayan, Y. A. Mowaqet, *Prog. Org. Coat.*, 2012, **75**, 456.
- P. B. Raja, M. Fadaeinasab, A. K. Qureshi, A. A. Rahim, H. Osman, M. Litaudon, K. Awang, *Ind. Eng. Chem. Res.*, 2013, **52**, 10582.
- P. M. Krishnegowda, V. T. Venkatesha, P. K. M. Krishnegowda, S. B. Shivayogiraju, *Ind. Eng. Chem. Res.*, 2013, **52**, 722.
- E. E. Oguzie, C. B. Adindu, C. K. Enenebeaku, C. E. Ogukwe, M. A. Chidiebere, K. L. Oguzie, *J. Phys. Chem. C*, 2012, **116**, 13603.
- H. Gerengi, H. I. Sahin, *Ind. Eng. Chem. Res.*, 2012, **51**, 780.
- S. A. Umoren, Z. M. Gasem, I. B. Obot, *Ind. Eng. Chem. Res.*, 2013, **52**, 14855.
- G. Ji, P. Dwivedi, S. Sundaram, R. Prakash, *Ind. Eng. Chem. Res.*, 2013, **52**, 10673.
- S. Garai, S. Garai, P. Jaisankar, J. K. Singh, A. Elango, *Corros. Sci.*, 2012, **60**, 193.
- P. Mourya, S. Banerjee, M. M. Singh, *Corros. Sci.*, 2014, **85**, 352.
- V. V. Torres, R. S. Amado, C. F. de Sá, T. L. Fernandez, C. A. Da Silva Riehl, A. G. Torres, E. D'Elia, *Corros. Sci.*, 2011, **53**, 2385.
- J. C. da Rocha, J. A. da Cunha Ponciano Gomes, E. D'Elia, *Corros. Sci.*, 2010, **52**, 2341.
- S. S. de Assunção Araújo Pereira, M. M. Pêgas, T. L. Fernández, M. Magalhães, T. G. Schöntag, D. C. Lago, L. F. de Senna, E. D'Elia, *Corros. Sci.*, 2012, **65**, 360.
- M. Lebrini, F. Robert, A. Lecante, C. Roos, *Corros. Sci.*, 2011, **53**, 687.
- L. J. Li, X. P. Zhang, J. L. Lei, J. X. He, S. T. Zhang, F. S. Pan, *Asian J. Chem.*, 2012, **24**, 1649.
- S. D. Deng, X. H. Li, *Corros. Sci.*, 2012, **55**, 407.
- N. Soltani, N. Tavakkoli, M. Khayatkashani, M. R. Jalali, A. Mosavizade, *Corros. Sci.*, 2012, **62**, 122.
- O. Rangasamy, G. Raelison, F. E. Rakotoniriana, K. Cheuk, S. Urverg-Ratsimamanga, J. Quetin-Leclercq, A. Gurib-Fakim, A. H. Subratty, *J. Ethnopharmacol.*, 2007, **109**, 331.
- M. S. Choi, M. S. Yoo, D. J. Son, H. Y. Jung, S. H. Lee, J. K. Jung, B. C. Lee, Y. P. Yun, H. B. Pyo, J. T. Hong, *J. Dermatol. Sci.*, 2007, **46**, 127.
- C. Y. Chen, L. Y. Huang, L. J. Chen, W. L. Lo, S. Y. Kuo, Y. D. Wang, S. H. Kuo, T. J. Hsieh, *Chem. Nat. Compd.*, 2008, **44**, 137.
- G. Gece, *Corros. Sci.*, 2008, **50**, 2981.
- G. Gece, *Corros. Sci.*, 2011, **53**, 3873.
- B. Sanyal, *Prog. Org. Coat.*, 1981, **9**, 165.
- R. Baskar, D. Kesavan, M. Gopiraman, K. Subramanian, *Prog. Org. Coat.*, 2014, **77**, 836.
- M. R. Heydarpour, A. Zarrabi, M. M. Attar, B. Ramezanzadeh, *Prog. Org. Coat.*, 2014, **77**, 160.
- D. Thirumoolan, V. A. Katkar, G. Gunasekaran, T. Kanai, K. A. Basha, *Prog. Org. Coat.*, 2014, **77**, 1253.
- M. Behpour, S. M. Ghoreishi, A. Gandomi-Niasar, N. Soltani, M. Salavati-Niasari, *J. Mater. Sci.* 2009, **44**, 2444.
- M. V. Fiori-Bimbi, P. E. Alvarez, H. Vaca, C. A. Gervasi, *Corros. Sci.*, 2015, **92**, 192.
- X. H. Li, S. D. Deng, H. Fu, G. N. Mu, *Corros. Sci.*, 2010, **52**, 1167.
- T. P. Zhao, G. N. Mu, *Corros. Sci.*, 1999, **41**, 1937.
- R. Baskar, D. Kesavan, M. Gopiraman, K. Subramanian, *RSC Adv.*, 2013, **3**, 17039.
- F. M. Donahue, K. Nobe, *J. Electrochem. Soc.*, 1965, **112**, 886.
- M. Shabani-Nooshabadi, M. Behpour, F. S. Razavi, M. Hamadani, V. Nejadshafiee, *RSC Adv.*, 2015, **5**, 23357.
- X. H. Li, S. D. Deng, H. Fu, *J. Appl. Electrochem.*, 2010, **40**, 1641.
- X. H. Li, S. D. Deng, H. Fu, G. N. Mu, *J. Appl. Electrochem.*, 2009, **39**, 1125.
- S. Manov, A. M. Lamazouere, L. Aries, *Corros. Sci.*, 2000, **42**, 1235.
- A. P. Srikanth, T. G. Sunitha, V. Raman, S. Nanjundan, N. Rajendran, *Mater. Chem. Phys.*, 2007, **103**, 241.
- F. Kandemirli, S. Sagdinc, *Corros. Sci.*, 2007, **49**, 2118.
- R. G. Pearson, *Inorg. Chem.*, 1988, **27**, 734.
- M. J. S. Dewar; W. Thiel, *J. Am. Chem. Soc.*, 1977, **99**, 4907.
- R. G. Parr; L. v. Szentpaly; S. Liu, *J. Am. Chem. Soc.*, 1999, **121**, 1922.
- V. S. Sastri; J. R. Perumareddi, *Corros. Sci.*, 1997, **53**, 617.
- I. B. Obot, N. O. Obi-Egbedi, *Colloid. Surface. A.*, 2008, **330**, 207.
- N. O. Eddy, B. I. Ita, *J. Mol. Model.*, 2011, **17**, 359.
- S. W. Xia, M. Qiu, L. M. Yu, F. G. Liu, H. Z. Zhao, *Corros. Sci.*, 2008, **50**, 2021.
- M. A. Amin, M. A. Ahmed, H. A. Arida, F. Kandemirli, M. Saracoglu, T. Arslan, M. A. Basaran, *Corros. Sci.*, 2011, **53**, 1895.
- H. Jafari, I. Danaee, H. Eskandari, M. RashvandAvei, *Ind. Eng. Chem. Res.*, 2013, **52**, 6617.
- L. M. Rodríguez-Valdez, A. Martínez-Villafañe, D. Glossman-Mitnik, *J. Mol. Struct. (THEOCHEM)*, 2005, **716**, 61.
- E. E. Oguzie, C. K. Enenebeaku, C. O. Akalezi, S. C. Okoro, A. A. Ayuk, E. N. Ejike, *J. Colloid. Interf. Sci.*, 2010, **349**, 283.
- Y. L. Li, Q. P. Qin, Y. C. Liu, Z. F. Chen, H. Liang, *J. Inorg. Biochem.*, 2014, **137**, 12.
- C. Y. Chen, S. Y. Chen, C. H. Chen, *Process. Biochem.*, 2012, **47**, 1460.
- D. Daoud, T. Douadi, S. Issaadi, S. Chafaa, *Corros. Sci.*, 2014, **79**, 50.
- M. Faustin, A. Maciuk, P. Salvin, C. Roos, M. Lebrini, *Corros. Sci.*, 2015, **92**, 287.
- G. Ji, S. Anjum, S. Sundaram, R. Prakash, *Corros. Sci.*, 2015, **90**, 107.
- M. S. Masoud, M. K. Awad, M. A. Shaker, M. M. T. El-Tahawy, *Corros. Sci.*, 2010, **52**, 2387.
- R. Goel, W. A. Siddiqi, B. Ahmed, M. S. Khan, V. M. Chaube, *Desalination*, 2010, **263**, 45.
- D. Özkır, K. Kayakırılmaz, E. Bayol, A. A. Gürten, F. Kandemirli, *Corros. Sci.*, 2012, **56**, 143.
- I. B. Obot, N. O. Obi-Egbedi, *Corros. Sci.*, 2010, **52**, 657.
- L. M. Rodríguez-Valdez, W. Villamizar, M. Casales, J. C. González-Rodríguez, A. Martínez-Villafañe, L. Martínez, D. Glossman-Mitnik, *Corros. Sci.*, 2006, **48**, 4053.
- M. S. Masoud, M. K. Awad, M. A. Shaker, M. M. T. El-Tahawy, *Corros. Sci.*, 2010, **52**, 2387.

- 67 J. J. Fu, H. S. Zang, Y. Wang, S. N. Li, T. Chen, X. D. Liu, *Ind. Eng. Chem. Res.*, 2012, **51**, 6377.
- 68 K. F. Khaled, M. A. Amin, *J. Appl. Electrochem.*, 2009, **39**, 2553.
- 69 K. F. Khaled, *J. Appl. Electrochem.*, 2011, **41**, 423.